

Rigidity-tuning conductive elastomer

Wanliang Shan^{1,3}, Stuart Diller^{1,3}, Abbas Tutcuoglu^{1,2} and Carmel Majidi¹

¹Department of Mechanical Engineering, Carnegie Mellon University, Pittsburgh, PA 15213, USA

²Department of Aeronautics, Imperial College London, London, UK

E-mail: cmajidi@andrew.cmu.edu

Received 25 October 2014, revised 28 January 2015

Accepted for publication 9 February 2015


Published DD MM 2015



CrossMark

Abstract

We introduce a conductive propylene-based elastomer (cPBE) that rapidly and reversibly changes its mechanical rigidity when powered with electrical current. The elastomer is rigid in its natural state, with an elastic (Young's) modulus of 175.5 MPa, and softens when electrically activated. By embedding the cPBE in an electrically insulating sheet of polydimethylsiloxane (PDMS), we create a cPBE–PDMS composite that can reversibly change its tensile modulus between 37 and 1.5 MPa. The rigidity change takes ~ 6 s and is initiated when a 100 V voltage drop is applied across the two ends of the cPBE film. This magnitude of change in elastic rigidity is similar to that observed in natural skeletal muscle and catch connective tissue. We characterize the tunable load-bearing capability of the cPBE–PDMS composite with a motorized tensile test and deadweight experiment. Lastly, we demonstrate the ability to control the routing of internal forces by embedding several cPBE–PDMS 'active tendons' into a soft robotic pneumatic bending actuator. Selectively activating the artificial tendons controls the neutral axis and direction of bending during inflation.

 Online supplementary data available from stacks.iop.org/sms/0/000000/mmedia

Keywords: rigidity tuning, conductive elastomer, artificial muscle

SQ1 (Some figures may appear in colour only in the online journal)

1. Introduction

Rapid and reversible change in mechanical rigidity has a central role in nature, from muscle-powered motor tasks and sexual reproduction to spontaneous change in shape for predator evasion. Organisms typically perform rigidity tuning with striated muscle tissue [13, 14] or hydrostatic skeletons [15]. In echinoderms, such as the sea cucumber, mechanical rigidity can also be controlled with catch connective tissue, which is composed of a network of relatively inextensible collagenous fibers in a soft protoglycemic gel [21, 31]. These natural composites and structures are lightweight and require ~ 0.1 – 1 s to change their tensile rigidity by 1–2 orders of magnitude. Such properties are essential in order for an organism to perform mechanical work, support heavy loads, and control internal stress distributions while still preserving their mechanical versatility.

Rigidity tuning also has a potentially central role in engineered systems, particularly in the areas of robotics and

wearable technologies. Recently, there has been growing interest in 'soft' robotics and related 'soft-matter' technologies composed almost entirely of elastomers, gels, fluids, colloidal suspensions, and other soft matter [17]. In contrast to conventional machines and electronics that are composed of permanently rigid materials, these soft machines exhibit many of the same elastic and rheological properties of their natural biological counterparts. Elasticity and mechanical versatility is essential for not only biomimetic/bioinspired multi-functionality but also for mechanical 'impedance' matching with natural human tissue for safe human-machine interaction. Whereas rigid materials constrain natural human motion and can cause bodily injury, soft materials preserve the natural mechanics of the host and distribute load to avoid high stress concentrations during impact.

However, as in natural organisms, an apparent *paradox* arises when using soft materials for performing motor tasks in soft or wearable robotics. The maximum mechanical stress that an elastic material can support is approximately proportional to its elastic (Young's) modulus (E). Therefore, an elastomer with a modulus of 1 MPa can only exhibit

³ Co-first authors: WS and SD contributed equally to this work.

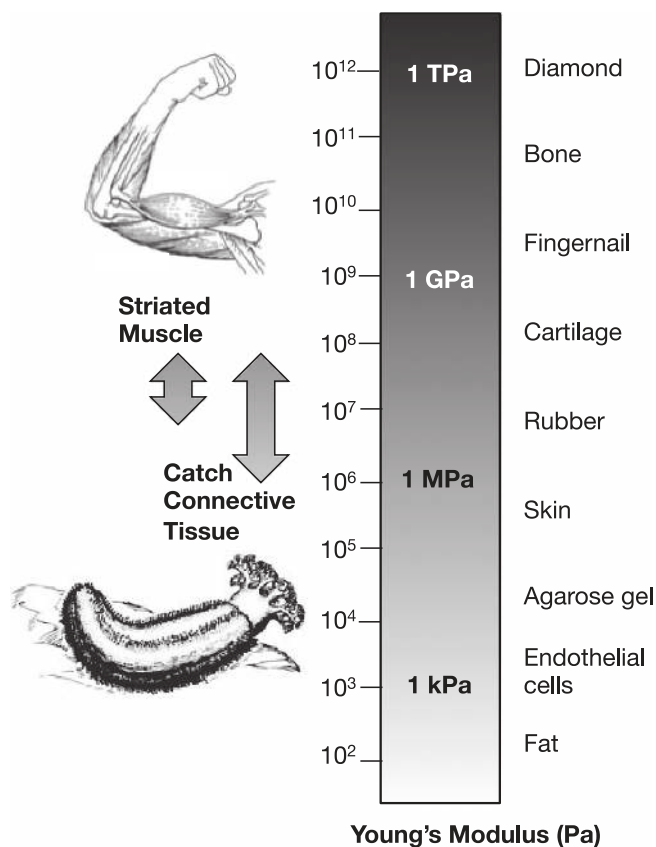


Figure 1. Young's modulus (E) of various materials in nature. Striated muscle and catch connective tissue exhibit the ability to reversibly change elastic modulus between 1–10 and 50 MPa, representing the difference in rigidity between skin and cartilage. Scale bar adapted from [1].

approximately 1/1000th the load-bearing capability of a rigid plastic (~ 1 GPa). Nature deals with this challenge through materials like muscle and catch connective tissue that actively change their elastic rigidity by tuning the internal sliding friction between inextensible myofilaments and collagen fibers, respectively. Referring to figure 1, the effective modulus E changes reversibly between ~ 10 and 50 MPa for striated muscle [13, 14] and ~ 1 and 50 MPa for echinoderm collagenous tissues [31]. This roughly corresponds to the difference in modulus between natural (latex) rubber and cartilage. While such metrics for rigidity are crude approximations that ignore nonlinear elasticity and viscous effects, they nonetheless demonstrate the scale and range of rigidity tuning that organisms and bio-inspired systems require for mechanical multi-functionality.

Here, we address the seemingly paradoxical requirement for soft materials to be load bearing by introducing a conductive propylene-based elastomer (cPBE) that reversibly changes its rigidity when activated with electric current (figure 2). When embedded in an electrically insulating sheet of polydimethylsiloxane (PDMS), the cPBE–PDMS composite can reversibly change its tensile modulus between ~ 1 and 100 MPa, thus exceeding the rigidity tuning properties of natural skeletal muscle and catch connective tissue. In contrast to previous materials and mechanisms for engineered

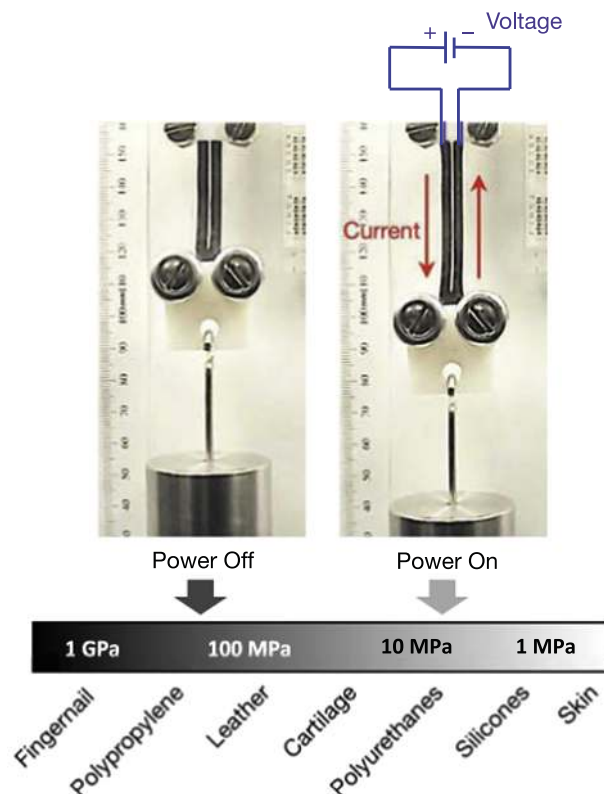


Figure 2. Abiotic rigidity tuning is accomplished with an elastomeric composite composed of conductive propylene-based elastomer (cPBE) embedded in polydimethylsiloxane (PDMS). When activated with electrical current, the cPBE rapidly and reversibly softens to 1–10% of its initial elastic rigidity.

rigidity tuning, this composite uniquely exhibits the following combination of properties:

- (i) *Electrically powered*—does not rely on bulky external hardware like fluidic pumps, air compressors, electromagnets, or motors.
- (ii) *Rapid and reversible*—changes modulus in *seconds* with moderate electrical power.
- (iii) *Scalable/patternable*—lightweight, inexpensive, and can be patterned with a CO₂ laser into any shape or circuit geometry.
- (iv) *Dramatic rigidity change*—depending on the volume fraction (χ) of cPBE to PDMS, the relative change (Γ) in elastic rigidity can range from $\times 10$ – 10^3 .

The tunable load-bearing capability of the cPBE–PDMS composite is examined with a motorized tensile test and deadweight experiment. Electrical current is used to control the elongation of the composite under prescribed uniaxial tensile loading. We also demonstrate the ability to route internal forces by integrating several cPBE–PDMS elements with a soft robotic inflatable bending actuator. Selectively powering these ‘active tendon’ elements controls the neutral axis and direction of bending during inflation.

Table 1. Comparison between different design approaches for multifunctional materials with tunable rigidity by recent studies using thermal approaches. Acronyms: ATR = activation time reported; RCF = rigidity change factor; SMP = shape memory polymer; LMPA = low-melting-point alloy; TP = thermoplastic; GT = glass transition.

Reference	Material	ATR (s)	Mechanism	RCF	Activation	Deformation mode
Haines <i>et al</i> [11]	Nylon	<1	GT	N.A.	External	Tensile and torsional
Capadona <i>et al</i> [5]	EO-EPI/whiskers	N.A.	Hydration	10 ²	External	Tensile
Capadona <i>et al</i> [5]	PVAc/whiskers	600	Melting	10 ³	External	Tensile
McKnight <i>et al</i> [20]	SMP	100	GT	100	External	Bending
Shan <i>et al</i> [26, 27]	SMP and elastomer	80	GT	100	Embedded	Bending
Shan <i>et al</i> [26, 27]	LMPA	60	Melting	10 ⁴	Embedded	Tensile and bending
Schubert <i>et al</i> [25]	LMPA	<1	Melting	25	<i>Direct</i>	Bending
McEvoy <i>et al</i> [19]	TP	5	Melting	100	Embedded	Bending
Cheng <i>et al</i> [8]	Wax and TP	>300	Melting	100	External	Compressive
Balasubramanian <i>et al</i> [3]	TP	2	GT	100	External	Tensile and bending
<i>Current Work</i>	cPBE	6	Softening	100	<i>Direct</i>	Tensile and Bending

2. Background

As engineering increasingly relies on non-rigid and multifunctional materials, there continues to be growing interest in rigidity-tuning composites. These include mechanical stiffness and damping/vibration control for reconfigurable morphing structures [9, 12, 32], active orthoses [6, 24], universal robotic grippers [4], and artificial muscles for soft and biologically-inspired robots [7, 10, 11, 19, 25, 26]. As with their natural counterparts, rigidity-tunable composites and systems should be self-contained, scalable/miniaturizable, lightweight ($\sim 1000 \text{ kg m}^{-3}$), and exhibit rapid ($\sim 0.1\text{--}1 \text{ s}$), reversible, and dramatic ($> 10\times$) changes in stiffness. Ideally, the composite should be electrically powered with the same circuitry, currents, and voltages typically used in microelectronics and have limited or no dependency on bulky external hardware for electrostatic, thermal, pneumatic, or hydraulic activation. Examples of external hardware used in rigidity tuning include pumps and valves for gel hydration [5, 8, 11, 28] or pneumatic particle jamming [4, 30], bulky electromagnets for activating magnetorheological fluids and elastomers [6, 18, 32], and high voltage activation for electroactive polymers [12]. While appropriate for relatively large machinery, these mechanisms cannot be easily scaled for clothing-embedded technologies, milli-robotics, and other applications that depend on miniaturization and autonomous operation.

Recently, there have been a series of efforts with thermal activation of non-conductive shape memory polymer (SMP) [3, 9, 20, 26], thermoplastics [19], coiled fibers [11], wax-soaked thermoplastics [8], and low-melting-point alloys (LMPA) [25, 26] using an external Joule heating element or through self (direct) Joule heating. These are summarized in table 1. Based on the rigidity tuning mechanisms, these composites can be categorized into two main mechanisms: phase change (melting) and glass transition. Activation is accelerated with an embedded electrical (ohmic, Joule) heating element that remains conductive during extreme bending and stretch deformations. This can be accomplished with microfluidic channels of liquid-phase metals, such as

gallium–indium (GaIn) alloy [26]. While promising, the use of liquid GaIn introduces sealing issues and requires separation from the thermally-responsive material, adding additional layers and sources of heat dissipation to the composite.

3. Materials and methods

As shown in steps (i) and (ii) of figure 3, the cPBE is produced by combining a propylene-ethylene co-polymer with a percolating network of structured carbon black. It has a weight composition of 51/9/40% propylene, ethylene and structured carbon black. Custom-ordered pellets are supplied by THEMIX Plastics, Inc (Lake Mills, WI) and pressed between steel plates at 90 °C to form thin sheets. Flattened sheets of cPBE (step iii) are patterned with a CO₂ laser to form shapes with electrical terminals to supply current (step iv). This final patterning step is accomplished using the method presented in figure A1 of the supplementary information.

Rigidity tuning measurements are performed on a composite that has total dimensions of 40 × 7.5 × 1.25 mm and contains a single U-shaped 2 × 0.65 mm strip of cPBE with a total length of 78 mm. Stress–strain curves for the unactivated composite, activated composite, and homogenous PDMS, and homogenous cPBE are measured using an Instron® materials tester (33R 4467). Using a least-squares algorithm, the curves for the PDMS dogbone samples, cPBE dogbone samples, and unactivated composites are fitted with a five-term expansion of the Ogden model for uniaxial stress: [22]

$$\sigma_{\text{Ogden}} = \sum_{p=1}^{n=5} \mu_p (\lambda^{2p} - \lambda^{-p}). \quad (1)$$

In contrast, stress–strain data for the activated composites were fitted with a line. The effective Young's moduli E_{eff}^{β} of the cPBE, PDMS, and composites were determined by averaging the moduli derived from the measured stress–strain curves. Here, the superscript $\beta \in \{n, a\}$ denotes whether the composite is non-activated and at room temperature (n) or activated with the cPBE heated above its transition

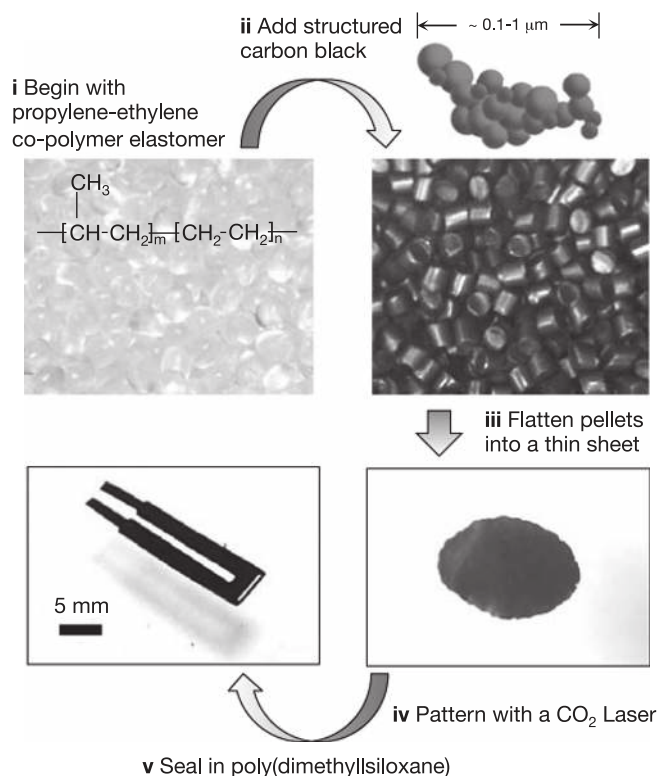


Figure 3. Fabrication of cPBE–PDMS composite: (i)–(ii) propylene-ethylene co-polymer (clear pellets) is mixed with structured carbon black to produce a conductive propylene-based elastomer (cPBE; black pellets); (iii)–(v). When flattened into thin sheets, the cPBE may be patterned with a CO₂ laser and embedded in PDMS.

temperature, i.e. softening point, T_s (a). Additional details are presented in the supplementary information.

The dependence of cPBE volumetric resistivity on temperature is determined using the procedure previously presented in [2]. Samples are placed in a temperature controlled oven (Thermo Scientific 664) and electrical resistance is determined with a multimeter (Agilent 34401A). Resistance-temperature measurements performed on two $33.5 \times 5.58 \times 0.68$ mm appear to be in reasonable agreement.

The soft pneumatic finger is composed of PDMS ‘phalanges’, soft silicone elastomer joints, and cPBE tendons. The PDMS and soft silicone are composed of Sylgard 184 (Dow Corning, Inc.) and Ecoflex 0030 (Smooth-on, Inc.), respectively. Both segments are produced with elastomer casting using 3D printed molds (Objet 24; Stratasys, Ltd.). After curing, the PDMS and Ecoflex segments are attached and a tube is inserted into the bottom. Next, U-shaped cPBE tendons are attached to the top and bottom segments of PDMS using uncured PDMS as an adhesive. A voltage of 150 V was applied across each of the cPBE tendons during activation, achieving full softening within 10 s. Various activation times were observed due to variations in the electrical contact resistances associated with the interface between the copper leads and the cPBE. This contact resistance may be due to a combination of stray PDMS insulating pieces and poor geometric conformance of the leads.

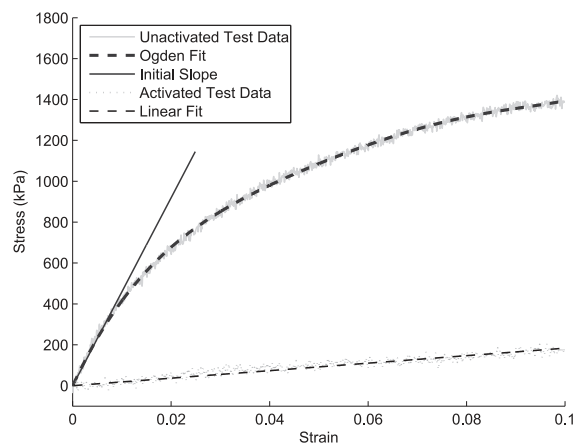


Figure 4. Representative stress–strain curves of a cPBE–PDMS sample during tensile loading with an Instron® tester: (solid) non-activated, (dashed) activated with electrical current.

4. Results

Referring to figure 3, the rigidity-tuning composite is composed of a laser-patterned conductive propylene-based elastomer (cPBE) embedded in an electrical and thermally-insulating sheet of PDMS. The cPBE is a composite of structured carbon black and propylene-ethylene co-polymer, which together form a conductive thermoplastic elastomer that heats and softens when electrical current is supplied. Fabrication is performed with a laser patterning method adapted from previous techniques developed for producing soft-matter circuits with carbon-based conductive PDMS (cPDMS) and liquid-phase eutectic gallium–indium (EGaIn) metal alloy [16]. Details of the laser patterning steps are presented in figure A1 of the appendix.

Representative stress–strain results for a single pair of activated and non-activated cPBE–PDMS composite tests are presented in figure 4. Based on the tensile testing results for all of the samples, $E_{\text{eff}}^n = 36.8$ MPa (st. dev. = 9.0 MPa) and $E_{\text{eff}}^a = 1.49$ MPa (st. dev. = 0.44 MPa). This represents a $\Gamma = 25\times$ change in tensile rigidity. For illustration, this is approximately the same as the difference between leather and a rubber band. The values $E_{\text{cPBE}} = 175.5$ MPa (st. dev. = 23.7 MPa) and $E_{\text{PDMS}} = 1.041$ MPa (st. dev. = 0.188 MPa) correspond to the Young’s modulus of the cPBE and PDMS at room temperature, respectively, and are independently obtained from tensile tests performed on homogeneous material specimens. We did not observe significant influence of the loading rate on the measured elastic modulus (see appendix).

A key feature of the cPBE is its ability to maintain conductivity even in its softened state. As shown in figure 5, electrical resistance was observed to increase exponentially with increasing temperature. Above a softening temperature of $T_s = 75$ °C, the contact area with the electrical terminals changes and the estimates of the electrical resistance are no longer reliable. Nonetheless, the roughly one order of magnitude increase in electrical resistivity is advantageous because it results in a self-limiting reduction in electrical

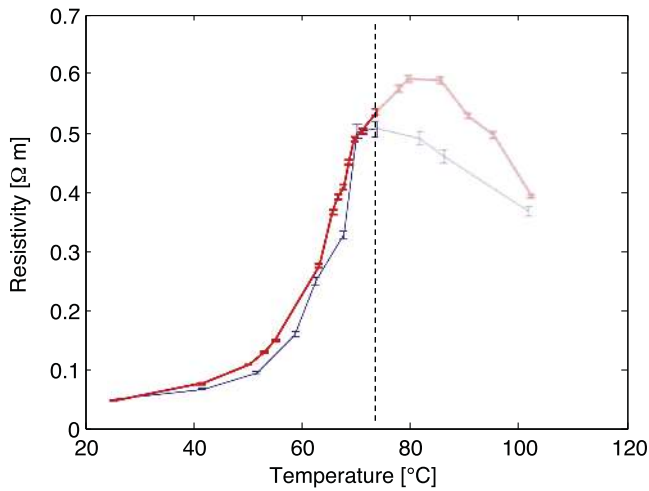


Figure 5. Electrical resistivity measured as a function of temperature for two $33.5 \times 5.58 \times 0.68$ mm samples of cPBE. Measurements are not reliable for temperatures above the 75°C transition point.

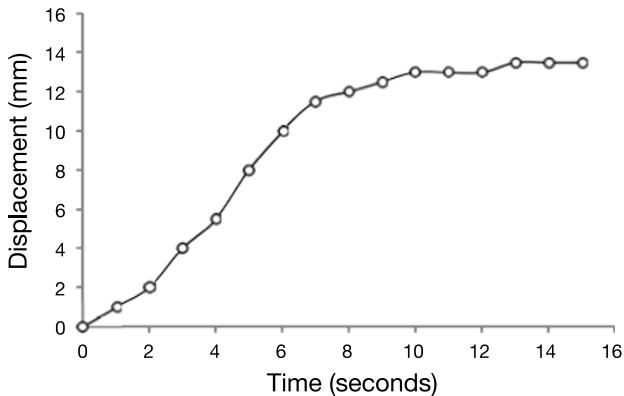
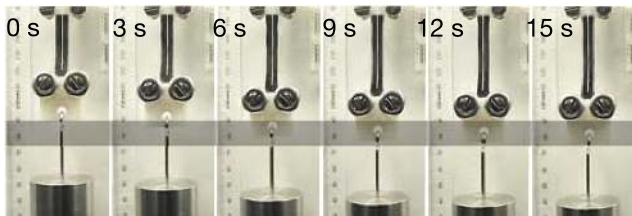


Figure 6. Extension of a cPBE–PDMS sample during 15 s of activation. The sample has dimensions of $34 \times 7.5 \times 1.25$ mm extends roughly 40% within a few seconds under an applied dead weight of 0.5 kg. (See video in *supplementary information*.)

power delivered to the sample when a fixed voltage is applied. This prevents burning or degradation of the cPBE and eliminates the need for timed activation or control.

To estimate the activation time, we examined the elongation of a cPBE–PDMS composite under a deadweight loading. As shown in figure 5, a sample supporting a 0.5 kg weight ($P = 4.9$ N) elongates by approximately 40% within seconds of activation. The sample is activated with approximately 0.17–3.3 W of electrical power under 100 V of fixed voltage (resistance increased from 3 to 60 k Ω and current decreased from 33 to 1.7 mA). Displacement appears to increase linearly with time for approximately 6–7 s.

Subsequently, the sample exhibits creep for several seconds as the displacement converges to its final value of 13 mm. The sample has a length $L = 34$ mm, cross-sectional area $A = 9.38$ mm², and cross-sectional area fraction $\chi = 0.277$ of cPBE. A displacement $u = 13$ mm implies that the composite has an effective modulus of $E_{\text{eff}}^a = PL/uA = 1.4$ MPa. This is consistent with measurements obtained for motorized tensile testing (figure 4).

Lastly, we demonstrate the potential to apply the cPBE–PDMS in soft robotics by integrating the composite with a pneumatic bending actuator. Referring to figure 7, the cPBE–PDMS composite is incorporated into a biomimetic soft robotic finger composed of PDMS phalanges connected by soft silicone (Ecoflex 0030; Smooth-On, Inc.) joints. Rigidity-tuning elements are attached to the outside of the hollow finger and control the ability of each side of the joints to extend when compressed air is delivered to the finger. By electrically tuning the elastic rigidity of the outer cPBE ‘artificial muscles’, the finger is capable of bending in different directions with just a single air supply and pneumatic tube figures 7(b)–(d).

5. Discussion

We present a novel approach to elastic rigidity tuning with a composite that contains laser-patterned layers of a cPBE embedded in an insulating PDMS seal. Because the cPBE is elastomeric and conductive, it can be directly heated with electrical current and stretched without mechanical or electrical failure. In contrast, SMPs, LMPA, thermoplastics, waxes, and other brittle or non-conductive thermally-responsive materials require a separate Joule heating element that must remain electrically functional during elastic deformation and mechanical load.

When heated to a transition temperature of $T_s = 75^\circ\text{C}$, the cPBE softens dramatically and the effective tensile modulus of the composite decreases. This change in rigidity is reversible and can be controlled in seconds by applying a voltage drop across either the faces or terminal ends of a flat cPBE strip. As with conductive PDMS (cPDMS) and other conductive elastomers, cPBE may be rapidly patterned with a CO₂ laser [16]. This allows for any planar geometries with ≥ 100 μm feature sizes to be produced in seconds. To achieve smaller features, the cPBE must be patterned with either a UV laser micromachining systems or through replica casting using a micromachined mold.

The rigidity change Γ can be controlled by the area fraction $\chi = A_{\text{cPBE}}/A$, which is defined as the ratio of the cross-sectional area of the embedded cPBE element (A_{cPBE}) to that of the composite (A). For the composite samples tested, $A_{\text{cPBE}} = 2 \times (2 \text{ mm}) \times (0.65 \text{ mm}) = 2.6 \text{ mm}^2$, $A = (7.5) \times (1.25 \text{ mm}) = 9.375 \text{ mm}^2$, and $\chi = 0.277$. In general, Γ is expected to be approximately

$$\Gamma = \frac{E_{\text{eff}}^n}{E_{\text{eff}}^a} = \left(\frac{\chi}{1 - \chi} \right) \frac{E_{\text{cPBE}}}{E_{\text{PDMS}}} + 1, \quad (2)$$

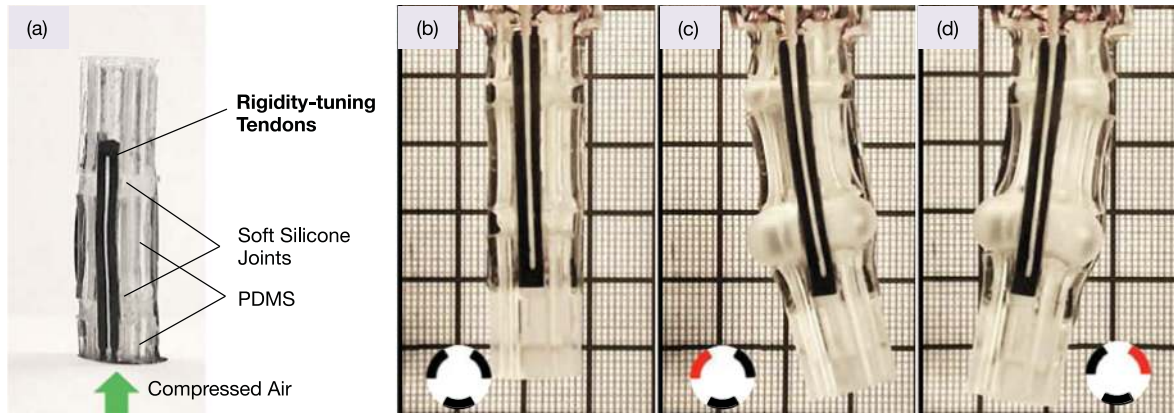


Figure 7. (a) Soft pneumatic robot finger integrated with cPBE ‘tendons’ and a single air supply, (b) at rest, not inflated and not activated (c)–(d) the finger bends in different directions depending on which tendon element is activated to allow for stretch. (See video in *supplementary information*.)

where $E_{\text{eff}}^n = \chi E_{\text{cPBE}} + (1 - \chi) E_{\text{PDMS}}$ and $E_{\text{eff}}^a = (1 - \chi) E_{\text{PDMS}}$ are the effective tensile moduli of the non-activated and activated composite, respectively. This approximation for Γ assumes that the activated cPBE has negligible stiffness and is therefore undefined in the limit as $\chi \rightarrow 1$. Prior to activation the composite is expected to have an effective modulus of $E_{\text{eff},n} = \chi E_{\text{cPBE}} + (1 - \chi) E_{\text{PDMS}} = 49.4 \text{ MPa}$, and prediction for the activated modulus is $E_{\text{eff}}^a = 0.753 \text{ MPa}$. According to (2), the corresponding rigidity of the composites tested in figure 2 is expected to be $\Gamma = 66\times$, compared with an averaged measured value of $25\times$. The predicted value for the activated modulus of the cPBE–PDMS composite is a factor of two lower than the measured value, and the predicted unactivated modulus is a factor of 1.5 higher. We attribute the discrepancies for the activated case to incomplete activation, possibly as a result of heat conduction from the sample to the metal clamps. We expect that the measured modulus is less stiff compared to theory because of manufacturing errors and incomplete merging of the plastic pellets, which creates ‘grain’ boundaries within the patterned cPBE. Improved manufacturing and design of the composite should lead to better performance and agreement with theory.

The results presented in figure 7 demonstrate a potential application in soft robotics. The observed deflections are modest and a more dramatic change in bending direction can be achieved with improvements to the design of the soft silicone joints. Nonetheless, this prototype clearly demonstrates one possible role of conductive thermoplastic elastomers for rigidity tuning in soft robotics and inflatable structures. Rather than requiring multiple air chambers and pneumatic tubing to control the bending direction, the finger has a single chamber and tube and multiple rigidity tunable elements that control the neutral axis of bending. Replacing pneumatic tubing and valves with electrical wiring can dramatically reduce the size and weight of soft robots and allows for simpler and more size-scalable geometries.

Future design improvements to reduce activation time and energy consumption can be informed by theoretical modeling. In particular, numerical solutions to the governing transient heat equation for an elastomeric composite can

provide predictions for the activation time and internal temperature distribution as a function of composite geometry and applied voltage. To examine this, we have performed a preliminary finite volume simulation (see appendix) and reported the results in the figure A2. For the selected cPBE–PDMS geometry, we find that it takes approximately 2 and 4 s for the cPBE to heat above T_s for applied voltages of 150 V and 100 V, respectively. As expected, temperature is greatest at the mid-plane of the composite and decreases smoothly and monotonically towards the surface. For example, with a voltage of 150 V, the temperature at the boundary is approximately 65°C at the time of complete activation. Moreover, for high input voltages the temperature in the cPBE domain is significantly higher than in the PDMS layer, due to the relatively fast heating. This temperature gradient is less pronounced at lower voltages, which has important implications for applications involving contacting with human skin. Lastly, we observe that activation time decreases significantly with a higher volume % of cPBE and/or lower film thickness. In contrast, the surface temperature at the time of complete activation of the cPBE is minimized for higher sample thicknesses and a lower fraction of cPBE. This can be attributed to an improved thermal insulation due to the thicker PDMS seal.

6. Concluding remarks

In this study, we introduce a rigidity-tuning composite composed of laser-patterned sheets of cPBE embedded in PDMS. When powered with electrical current, the cPBE heats up and softens when the temperature exceeds a critical softening point of approximately $T_s = 75^\circ\text{C}$. With $\sim 0.1\text{--}1 \text{ W}$ of supplied electrical power, the effective elastic modulus of the composite reversibly changes between 1.5 and 37 MPa. This approximately corresponds to the difference in rigidity between human cartilage and skin. A central feature of the composite is the resistance of the embedded cPBE to fracture. While LMPA and carbon-filled thermoplastics or waxes can also be directly heated with electrical current, they are

susceptible to brittle failure when in their rigid state and this can prevent initial activation. While such materials may be appropriate for reversibly changing flexural rigidity [25], they cannot be used in applications that require changes in *tensile* rigidity. Finally, soft robot integration is demonstrated with a pneumatic bending actuator capable of motion in multiple directions with a single pneumatic actuator. Future work will explore further implementation of cPBE–PDMS composites as ‘active tendons’ in soft robot artificial muscles and load-bearing reconfigurable structures. Additionally, testing of the rheology of cPBE could better inform theoretical models of composite behavior, and subsequently improve the design of devices and agreement with experimental measurements.

Acknowledgments

This work is supported by Defense Advanced Research Projects Agency (DARPA) Young Faculty Award (Grant no. N66001-12-1-4255). The authors hereby would also like to acknowledge the helpful discussions with Mr Steven Kidd from THEMIX Plastics, Inc, in manufacturing of cPBE.

Appendix

cPBE patterning: the cPBE is composed of a 51/9/40 wt% of propylene, ethylene and structured carbon black. Pellets are supplied by THEMIX Plastics, Inc (Lake Mills, WI) and pressed between steel plates at 90 °C to form thin sheets. Next, the sheets are patterned with a 30 W CO₂ laser engraver (VLS 3.50; Universal Laser Systems) and embedded in PDMS (Sylgard 184; Dow Chemicals) using the procedure presented in figure A1. This is adapted from rapid prototyping techniques developed for patterning thin layers of cPDMS and liquid-phase EGaIn metal alloy [16]. As shown in the figure, we begin with a brass cutting sheet that is then covered with a sheet of cPBE. After patterning with the CO₂ laser engraver, the excess cPBE is removed and the elastomer is sealed in PDMS. The composite has total dimensions of 40 × 7.5 × 1.25 mm and contains a single U-shaped 2 × 0.65 mm strip of cPBE that has a total length of 78 mm.

Measuring elastic modulus: representative stress–strain curves for a non-activated and activated characteristic PDMS–cPBE sample are presented in figure 4. Samples are loaded in tension using an Instron® materials tester (model number: 33R 4467) with a model with a 30 kN Instron load cell (Cat. # 2716-015). Dogbone samples of homogeneous PDMS and homogeneous cPBE were also tested in tension to obtain the elastic modulus of each material independently. Using a least-squares algorithm, the curves for the PDMS dogbones, cPBE dogbones, and unactivated composites are fitted with a five-term expansion of the Ogden model. In these cases, the *effective* Young’s modulus is determined by averaging the slope of the Ogden curve between approximately 0.2 and 0.3% strain to avoid inaccurate curvature of the fit at the origin. For the cPBE dogbones and the unactivated



Figure A1. Steps for fabrication: (i) start with a flat cutting substrate, (ii) cover with a layer of cPBE, (iii) pattern with a CO₂ laser, (iv) remove excess material, (v) seal with PDMS, (vi) pattern edges and release.

composites, the Ogden curve was fit to the first 1% of strain for the purpose of determining the elastic modulus to decrease the overall least squared value. For the PDMS dogbones, the Ogden curve was fit to the first 5% of strain to mitigate noise in the stress values. The elastic modulus of the activated composites was determined by fitting a linear curve to the entirety of the data (up to 30% strain). This technique was used because noise in the force measurements prevented reliable measurement of slope near the origin, and because the activated composite curves appeared to be approximately linear. In total, five PDMS dogbones were tested at loading rates of 5, 20, and 50% min⁻¹ for a total of 15 tests. Likewise, four cPBE dogbones were tested at loading rates of 1, 5, 10, and 20% min⁻¹, and four composite samples were tested at loading rates of 2, 5, 10, 20, and 50% min⁻¹ while unactivated, and at 2 and 20% min⁻¹ while activated.

Transient heat analysis: the transient heat analysis is adapted from a technique previously used to examine heat transfer in rigidity tunable composites composed with SMP and LMPA along with a serpentine channel of liquid-phase GaIn alloy for Joule heating [27]. Using a finite volume method, we examine heat transfer within a 34 mm long and 4 mm wide composite that contains a 0.7 mm thick layer of cPBE sandwiched between two 0.3 mm thick layers of PDMS. When simulating the temperature distribution within an activated cPBE–PDMS composite, we assume constant specific heat coefficient c_p , density ρ , and thermal conductivity κ . Because of the dependency of electrical resistivity on temperature, we must let the heat generation q also be temperature-dependent. The main challenge of this analysis lies in the non-continuous change in material properties at the

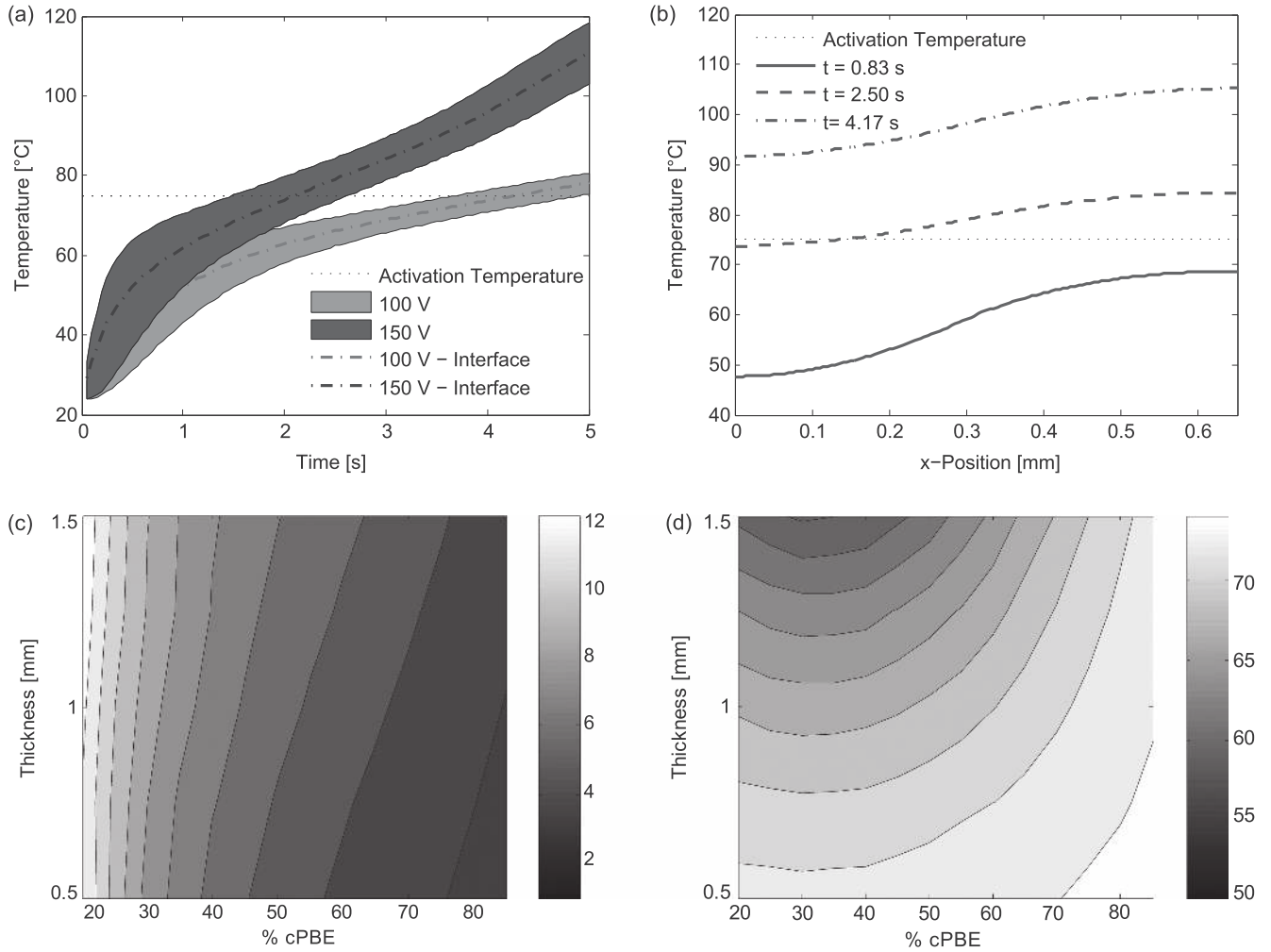


Figure A2. (a) Theoretically predicted temperature versus time for 100 V (*gray*) and 150 V (*black*) of applied voltage; bottom and top lines correspond to the composite surface and midplane, respectively, and the dashed line corresponds to the cPBE–PDMS interface. (b) Temperature distribution across the sample thickness for 150 V of applied voltage. Contour plots for (c) activation time in seconds and (d) boundary temperature in Celsius as functions of composite thickness and percentage cPBE for 100 V of applied voltage. These contour plots are used to determine the composite film thickness and cPBE volume fraction required to achieve a desired activation time and surface temperature for the following fixed values: composite length = 34 mm, composite width = 4 mm, end-to-end voltage drop = 100 V.

interface of cPBE and PDMS, requiring special treatment of the numerical formulation of the transient nonlinear heat transfer equation:

$$\begin{aligned} \frac{\partial}{\partial x} \left\{ \kappa(x) \frac{\partial T}{\partial x} \right\} + q(x, T) \\ = \rho(x) c_p(x) \frac{\partial T}{\partial t}, \end{aligned} \quad (3)$$

where $x \in \Omega$ is the spatial variable, t is time, T denotes temperature, $\Omega = [0, \ell]$, and ℓ is the sample thickness. The symmetry of the PDMS–cPBE–PDMS sandwich structure allows Neumann conditions to be imposed at the axis of symmetry. A finite volume approach is performed in which energy is conserved within each volumetric cell [29]. The vortex centered scheme defines the temperature at the set of nodes $\{x_i, | i \in \{0, \dots, N + 1\}\}$, which correspond to the center of control volumes K_i . The control volumes, in turn, are bounded by interfaces $\{x_{i+1/2} | i \in \{-1, \dots, N + 1\}\}$, which are placed at the center of their respective neighboring

nodes. The heat generation of K_i is calculated using Joule's first law $P = V^2/R(T)$, where $R(T)$ is the temperature dependent electrical resistance and can be expressed in the following manner:

$$R(T) = \frac{\rho_{el}(T)L}{(x_{i+1/2} - x_{i-1/2})w}, \quad (4)$$

where ρ_{el} denotes electric resistivity as measured in figure 5 and L and w are the sample's length and width, respectively. While both ρ and c_p are calculated at the nodes, conservation of energy requires the flux to be evaluated at the interfaces. This necessitates κ to be determined at the interfaces at each time step. Taking the average as $\kappa_{i+1/2} = 1/2(\kappa_i + \kappa_{i+1})$ yields a first-order accurate approximation in space [23]. An

explicit scheme is used to discretize equation (3):

$$(\rho c_p)_i (T_i - T_i^0) = \Delta t q_i + \frac{\Delta t}{\Delta x} \left\{ \kappa_{i+\frac{1}{2}} \frac{T_{i+1}^0 - T_i^0}{x_{i+1} - x_i} - \kappa_{i-\frac{1}{2}} \frac{T_i^0 - T_{i-1}^0}{x_i - x_{i-1}} \right\}. \quad (5)$$

Convection at the boundary is implemented using the following scheme [29]:

$$T_0 = \left(T_1 + \frac{T_{\text{air}} h_{\text{air}} \Delta x}{k_{\text{PDMS}}} \right) \left(1 + \frac{h_{\text{air}} \Delta x}{k_{\text{PDMS}}} \right)^{-1}. \quad (6)$$

References

- Q7
- [1] Autumn K, Majidi C, Groff R E, Dittmore A and Fearing R 2006 Effective elastic modulus of isolated gecko setal arrays *J. Exp. Biol.* **209** 3558–68
- Q2
- [2] Bak C 2012 *Resistivity: The Fine Art of Measuring Electrical Resistance* (Fabrico)
- [3] Balasubramanian A, Standish M and Bettinger C J 2014 Microfluidic thermally activated materials for rapid control of macroscopic compliance *Adv. Funct. Mater.* **24** 4860–6
- [4] Brown E, Rodenberg N, Amend J, Mozeika A, Steltz E, Zakin M R, Lipson H and Jaeger H M 2010 *Proc. Natl Acad. Sci. USA* **107** 18809–14
- [5] Capadona J R, Shammuganathan K, Tyler D J, Rowan S J and Weder C 2008 Stimuli-responsive polymer nanocomposites inspired by the sea cucumber dermis *Science* **319** 1370–4
- [6] Chen J Z and Liao W H 2010 Design, testing and control of a magnetorheological actuator for assistive knee braces *Smart Mater. Struct.* **19** 035029
- [7] Chenal T, Case J, Paik J and Kramer R K 2014 Variable stiffness fabrics with embedded shape memory materials for wearable applications *Proc. IEEE/RSJ Int. Conf. on Intelligent Robots and Systems*
- Q3
- [8] Cheng N G, Gopinath A, Wang L, Iagnemma K and Hosoi A E 2014 Thermally tunable, self-healing composites for soft robotic applications *Macromol. Mater. Eng.* doi:10.1002/mame.201400017
- [9] Clark W W, Brigham J C, Mo C and Joshi S 2010 Modeling of a high-deformation shape memory polymer locking link *Proc. SPIE Indust. Commercial Appl. Smart Struct* 7645
- Q4
- [10] Culha U, Nurzaman S G, Clemens F and Iida F 2014 Sensorization of soft structures with guidance of strain vectors *Sensors* submitted doi:10.3390/s140712748
- [11] Haines C S *et al* 2014 Artificial muscles from fishing line and sewing thread *Science* **343** 868–72
- Q5
- [12] Henke M, Sorber J and Gerlach G Multi-layer beam with variable stiffness based on electroactive polymers *Proc. SPIE Electroactive Polym. Actuators Devices* **8340** 83401P
- [13] Hunter I W and Lafontaine S 1992 A comparison of muscle with artificial actuators *IEEE Solid-State Sensor and Actuator Workshop* **5** 178–85
- [14] Jung D W G, Blange T, de Graaf H and Treijtel B W 1988 Elastic properties of relaxed, activated, and rigor muscle fibers measured with microsecond resolution *Biophys. J.* **54** 897–908
- [15] Kier W M 2012 The diversity of hydrostatic skeletons *J. Exp. Biol.* **215** 1247–57
- [16] Lu T, Finkenauer L, Wissman J and Majidi C 2014 Rapid prototyping for soft-matter electronics *Adv. Funct. Mater.* **24** 3351–6
- [17] Majidi C 2013 Soft robotics: a perspective-current trends and prospects for the future *Soft Robot.* **1** 5–11
- [18] Majidi C and Wood R J 2010 Tunable elastic stiffness with microconfined magnetorheological domains at low magnetic field *Appl. Phys. Lett.* **97** 164104
- [19] McEvoy M A and Correll N 2014 Thermoplastic variable stiffness composites with embedded, networked sensing, actuation, and control *J. Com. Mater.* **0** 1–10
- [20] McKnight G, Doty R, Keefe A, Herrera G and Henry C 2010 Segmented reinforcement variable stiffness materials for reconfigurable surfaces *J. Intelligent Mater. Syst. Struct.* **21** 1783–93
- [21] Motokawa T 1984 Connective tissue catch in echinoderms *Biol. Rev.* **59** 255–70
- [22] Ogden R W 1997 *Nonlinear Elastic Deformations* (New York: Dover)
- [23] Ozisik N 1994 *Finite Difference Methods in Heat Transfer* (Boca Raton, USA: CRC Press, Inc.)
- [24] Pratt G A and Williamson M M 1995 Series elastic actuators *Proc. IEEE/RSJ Conf. Intelligent Robots and Systems*
- [25] Schubert B E and Floreano D 2013 Variable stiffness material based on rigid low-melting-point-alloy microstructures embedded in soft poly(dimethylsiloxane) (pdms) *RSC Adv.* **3** 24671
- [26] Shan W L, Lu T and Majidi C 2013 Soft-matter composites with electrically tunable elastic rigidity *Smart Mater. Struct.* **22** 085005
- [27] Shan W L, Lu T, Wang Z H and Majidi C 2013 Thermal analysis and design of a multi-layered rigidity tunable composite *Int. J. Heat Mass Transfer* **66** 271–8
- [28] Shammuganathan K, Capadona J R, Rowan S J and Weder C 2010 Biomimetic mechanically adaptive nanocomposites *Prog. Polym. Sci.* **35** 212–22
- [29] Tao W 2001 *Numerical Heat Transfer* 2nd edn (Xi'an, China: Xi'an Jiaotong University Press)
- [30] Trappe V, Prasad V, Cipelletti L, Sergre P N and Weitz D A 2001 Jamming phase diagram for attractive particles *Nature* **411** 772–5
- [31] Trotter J A *et al* 2000 Towards a fibrous composite with dynamically controlled stiffness: lessons from echinoderms *Biochem. Soc. Trans.* **28** 357–62
- [32] Varga Z Z, Filipcsei G and Zrinyi M 2006 Magnetic field sensitive functional elastomers with tuneable elastic modulus *Polymer* **47** 227–33

QUERY FORM

JOURNAL: Smart Materials and Structures

AUTHOR: W Shan *et al*

TITLE: Rigidity-tuning conductive elastomer

ARTICLE ID: sms511436

The layout of this article has not yet been finalized. Therefore this proof may contain columns that are not fully balanced/matched or overlapping text in inline equations; these issues will be resolved once the final corrections have been incorporated.

SQ1

Please be aware that the colour figures in this article will only appear in colour in the online version. If you require colour in the printed journal and have not previously arranged it, please contact the Production Editor now.

Page

Q1

We have been provided funding information for this article as below. Please confirm whether this information is correct. Defense Advanced Research Projects Agency: N660011214255.

Page 9

Q2

Publisher location and name are required for book reference [2]. Please provide the missing information.

Page 9

Q3

Please update the volume and page range in reference [8].

Page 9

Q4

Please provide updated details for reference [10] if available.

Page 9

Q5

Please provide the year of publication in reference [12].

Page 9

Q6

Please provide the volume number in references [9, 16].

Page 9

Q7

Please check the details for any journal references that do not have a link as they may contain some incorrect information.
